Dynamic ^{18}F-FPCIT PET: Quantification of Parkinson Disease Metabolic Networks and Nigrostriatal Dopaminergic Dysfunction in a Single Imaging Session

Shichun Peng[1], Chris Tang[1], Katharina Schindlbeck[1], Yaacov Rydzinski[2], Vijay Dhawan[1], Phoebe G. Spetsieris[1], Yilong Ma[1]*, and David Eidelberg[1]*

[1]*Center for Neurosciences, Institute of Molecular Medicine, Feinstein Institutes for Medical Research, Northwell Health, Manhasset, New York; and* [2]*Department of Radiology, Icahn School of Medicine at Mount Sinai, New York, New York*

Previous multicenter imaging studies with ^{18}F-FDG PET have established the presence of motor-related and cognition-related metabolic patterns of Parkinson disease (PD), termed the PD-related pattern (PDRP) and the PD cognition–related pattern (PDCP), respectively, in patients with this disorder. Given that in PD cerebral perfusion and glucose metabolism are typically coupled in the absence of medication, we determined whether subject expression of these disease networks can be quantified in early-phase images from dynamic ^{18}F-*N*-(3-fluoropropyl)-2β-carboxymethoxy-3β-(4-iodophenyl)nortropane (^{18}F-FPCIT) PET scans acquired to assess striatal dopamine transporter (DAT) binding. **Methods:** We studied a cohort of early-stage PD patients and age-matched healthy control subjects who underwent ^{18}F-FPCIT at baseline; scans were repeated 4 y later in a smaller subset of patients. The early ^{18}F-FPCIT frames, which reflect cerebral perfusion, were used to compute PDRP and PDCP expression (subject scores) in each subject and were compared with analogous measures computed on the basis of the ^{18}F-FDG PET scan when additionally available. The late ^{18}F-FPCIT frames were used to measure caudate and putamen DAT binding in the same individuals. **Results:** PDRP subject scores from early-phase ^{18}F-FPCIT and ^{18}F-FDG scans were elevated and striatal DAT binding was reduced in PD versus healthy subjects. The PDRP scores from ^{18}F-FPCIT correlated with clinical motor ratings, disease duration, and corresponding measures from ^{18}F-FDG PET. In addition to correlating with disease duration and analogous ^{18}F-FDG PET values, PDCP scores correlated with DAT binding in the caudate or anterior putamen. PDRP and PDCP subject scores using either method rose over 4 y, whereas striatal DAT binding declined over the same period. **Conclusion:** Early-phase images obtained with ^{18}F-FPCIT PET can provide an alternative to ^{18}F-FDG PET for PD network quantification. This technique therefore allows PDRP/PDCP expression and caudate/putamen DAT binding to be evaluated with a single tracer in a single scanning session.

Key Words: Parkinson disease; cerebral perfusion; metabolic networks; dual-phase imaging; ^{18}F-FPCIT PET; ^{18}F-FDG PET

J Nucl Med 2021; 62:1775–1782
DOI: 10.2967/jnumed.120.257345

Parkinson disease (PD) is characterized by a widespread disruption of regional cerebral glucose metabolism and blood flow in response to degeneration of the nigrostriatal dopamine system and related pathways. Over the last 2 decades, a wide variety of imaging biomarkers has been developed for PD by measuring, first, striatal binding of presynaptic and postsynaptic dopaminergic markers such as dopamine transporter (DAT) and D_2 receptor using radioligands with both PET and SPECT; second, regional brain metabolism with ^{18}F-FDG PET; and third, regional brain perfusion with PET, SPECT, and arterial spin labeling MRI. Dopaminergic markers measure highly localized neurochemical deficits in the brain, whereas regional metabolism and blood flow provide versatile markers of functional activity at the network level (*1–4*).

It has been shown with ^{18}F-FDG PET in American populations that motor disability and cognitive dysfunction in PD are associated with highly reproducible disease-related metabolic covariance patterns termed the PD-related pattern (PDRP) (*5*) and the PD cognition–related pattern (PDCP) (6), respectively, both of which have since been replicated in multiple patient cohorts scanned in a variety of independent imaging centers in Asia and Europe (*4*,*7–11*). Expression levels for PDRP and PDCP in individual patients (subject scores) correlate with individual differences in motor and cognitive dysfunction. These measures increase with disease progression and correlate with striatal presynaptic dopaminergic markers in both cross-sectional (*10*,*12*,*13*) and longitudinal (*14*) investigations. More specifically, PDRP and PDCP expression values have been found to correlate with dopaminergic activity, respectively, in the posterior putamen and in the caudate and anterior putamen in a PET study using both ^{18}F-FDG and ^{18}F-FDOPA in the same patients (*15*). Indeed, subject scores for these patterns have been used to assess rates of disease progression and treatment responses in PD without the floor effects seen with presynaptic dopaminergic imaging markers (*16*).

PDRP and PDCP subject scores can be measured in cerebral blood flow images obtained with $H_2{}^{15}O$ PET and correlate strongly with analogous scores in concurrent ^{18}F-FDG PET scans in patients with PD (*5*,*17*). These early reports established high reproducibility of PDRP and PDCP subject scores in test–retest studies with both cerebral blood flow and metabolic images regardless of clinical stages and treatment status. This reproducibility suggests that perfusion scans can substitute for ^{18}F-FDG PET because of the tight coupling between these tracers that exists in the absence of dopaminergic medication at the regional and network levels (*18*,*19*).

Received Sep. 24, 2020; revision accepted Mar. 9, 2021.
For correspondence or reprints, contact Yilong Ma (yma@northwell.edu).
*Contributed equally to this work.
Published online March 19, 2021.

Subsequent studies have revealed that early-phase scans from dynamic PET imaging of dopaminergic tracers such as ^{11}C-raclopride provide measures of cerebral perfusion that can complement striatal D_2 receptor binding measurements from late-phase data (*20*). Indeed, a dynamic PET study with DAT radioligands such as *N*-(3-iodoprop-2E-enyl)-2β-carbomethoxy-3β-(4-methyl-phenyl)nortropane (^{11}C-PE2I) or ^{18}F-*N*-(3-fluoropropyl)-2β-carboxymethoxy-3β-(4-iodophenyl)nortropane (^{18}F-FPCIT) can provide a powerful alternative to dual-tracer or dual-modality examinations such as ^{123}I-FPCIT SPECT and ^{18}F-FDG PET used for the differential diagnosis of parkinsonism (*21*,*22*). To date, however, it is unclear whether such early-phase scans can be used (instead of ^{18}F-FDG PET) to quantify PDRP and PDCP expression in patients and healthy control subjects.

In this PET study, we determined, first, whether PDRP and PDCP expression levels can be quantified with early-phase ^{18}F-FPCIT scans (Can these measurements accurately discriminate PD patients from HC subjects?); second, how well these measures correlate with independent clinical ratings of disease severity; third, how well these values compare with corresponding expression levels determined independently with ^{18}F-FDG PET in the same subjects; fourth, what the relationships are between pattern expression and caudate and putamen DAT binding measurements obtained with dynamic ^{18}F-FPCIT PET in the same scanning session; and fifth, how well these pattern expression measures can track changes associated with disease progression.

MATERIALS AND METHODS

Human Subjects

Patients with early-stage PD without dyskinesia ($n = 25$) and age-matched heathy control (HC) subjects ($n = 16$) underwent dynamic ^{18}F-FPCIT PET as described elsewhere (*12*). In PD patients, imaging was conducted in the fasting state, at least 12 h after the last dose of antiparkinsonian medication; before imaging, patients were evaluated clinically according to Hoehn and Yahr stage and the Unified PD Rating Scale (UPDRS motor). Clinical and demographic details for these subjects are provided in Table 1. Of these participants, a subgroup of 18 PD and 7 HC subjects was additionally studied with ^{18}F-FDG PET under similar scan conditions, conducted within approximately 1 mo of ^{18}F-FPCIT PET. Of the patients scanned with ^{18}F-FPCIT and ^{18}F-FDG PET, 8 were rescanned after an average of 4 y (mean between-session interval, 46.4 ± 14.7 mo). The study was approved by the institutional review board of North Shore University Hospital. All subjects gave written informed consent after receiving a detailed explanation of the imaging procedures. The study complied with the Health Insurance Portability and Accountability Act.

Dual-Tracer PET Imaging

PET imaging studies were performed in 3-dimensional mode on a GE Healthcare Advance camera at North Shore University Hospital. ^{18}F-FPCIT images were acquired in dynamic mode over 0–100 min after injection. ^{18}F-FDG images were obtained in static mode over 35–45 min after injection on separate days. Both images were reconstructed using a 3-dimensional reprojection algorithm after attenuation correction with a PET transmission scan collected for each emission imaging session. Dynamic ^{18}F-FPCIT frames and static ^{18}F-FDG images were separately processed according to analytic protocols established at our center (*5*,*23*). Images of DAT binding were generated by a specific uptake ratio measured on late-phase ^{18}F-FPCIT PET defined by (voxel count/occipital count − 1) between 90 and 100 min after injection. Striatal DAT binding was then measured on a hemispheric basis and averaged in the caudate nucleus, the putamen, and its subdivisions using customized volumes of interest (VOIs) for each subject. The same set of VOIs was projected onto the DAT binding images in the follow-up analysis. All dynamic ^{18}F-FPCIT frames (via early-phase data) and ^{18}F-FDG images were spatially normalized to the PET template in SPM (Wellcome Department of Imaging Neurosciences, Institute of Neurology) implemented in Matlab, version 7.3.0 (MathWorks Inc.), and smoothed with a 3-dimensional gaussian kernel of 10-mm width to enhance the signal-to-noise ratio over the whole brain.

Network Expression

PDRP and PDCP expression levels (subject scores) were computed in early-phase dynamic ^{18}F-FPCIT PET scan frames and in the static ^{18}F-FDG images as described in detail elsewhere (*2*,*24*). These computations used an automated, voxel-based algorithm and were conducted with masking of the subject category (PD or HC), the radiotracer (^{18}F-FPCIT or ^{18}F-FDG), and the time window or time point. For all scans, subject scores were standardized (*z*-scored) with respect to the mean and SD of the HC group. The software used for these calculations

TABLE 1
Demographic and Clinical Characteristics of HC Subjects and PD Patients

Parameter	*n*	Age (y)	Sex (F/M)	HY stage	Duration (y)	UPDRS motor
^{18}F-FPCIT						
HC	16	52.8 ± 17.1	11/5	NA	NA	NA
PD	25	60.0 ± 10.8	6/19	1.6 ± 1.0	4.8 ± 4.9	12.2 ± 9.6
PD1	8	62.6 ± 7.1	0/8	1.2 ± 0.4	3.0 ± 3.1	8.4 ± 5.1
PD2*		66.4 ± 7.8		2.2 ± 0.4	6.8 ± 3.5	16.9 ± 5.0
^{18}F-FDG						
HC	7	59.3 ± 13.5	3/4	NA	NA	NA
PD	18	60.4 ± 9.0	4/14	1.3 ± 0.4	2.8 ± 1.7	9.4 ± 4.9
PD1	8	59.2 ± 8.0	1/7	1.2 ± 0.4	2.0 ± 1.3	9.6 ± 4.8
PD2*		63.0 ± 8.4		2.1 ± 0.4	5.8 ± 1.4	17.4 ± 4.9

*$P < 0.0001$, paired Student *t* tests of follow-up data compared with baseline.

HY = Hoehn and Yahr; UPDRS = unified PD rating scale; NA = not applicable.

PD1 and PD2 refer to baseline and 4-y scans of longitudinal PD group. Of 8 PD patients with follow-up, 7 had both ^{18}F-FPCIT and ^{18}F-FDG PET whereas the others underwent imaging with either tracer. Data are mean ± SD.

is freely available at http://www.feinsteinneuroscience.org/. To determine the optimal time window for early-phase imaging, we used linear interpolation to divide imaging frames of variable duration over the first 10 min after ^{18}F-FPCIT injection into 10 individual frames of 1-min duration and computed PDRP and PDCP subject scores individually for each frame (Supplemental Fig. 1; Supplemental Tables 1–2). This procedure also mitigated the effects of unequal framing in dynamic acquisitions commonly performed in clinical practice. Mean subject scores were then calculated by averaging over scan durations of 2, 5, and 10 min. Composite images (Fig. 1) were also displayed as the weighted average over the same frames to visualize regional cerebral perfusion across subject groups.

Statistical Analysis

Differences between 2 independent groups or within-subject changes between 2 dependent variables were assessed by unpaired and paired Student *t* tests, respectively. Differences in the rates of longitudinal change or in network expression values (subject scores) computed over the 3 specified ^{18}F-FPCIT time windows were compared using 1- and 2-way repeated-measures ANOVA models. Relationships between within-subject variables were evaluated in each group by Pearson correlation coefficients. Data were analyzed using SPSS software (SPSS Inc.) running on a Microsoft Windows Virtual PC, with the level of significance set at a P value of less than 0.05.

RESULTS

Optimal Time Window

PDRP subject scores computed in the individual 1-min frames over the first 10 min after ^{18}F-FPCIT injection provided similar discrimination of PD patients from HC subjects (Supplemental Fig. 1; Supplemental Tables 1–2). Additionally, network correlations of PDRP and PDCP scores with motor ratings, disease duration, and analogous ^{18}F-FDG PET measures were of comparable magnitude across the individual frames. Longitudinal changes in subject scores over the 4-y follow-up period were also similar for the various frames. The optimal time window was determined by comparing the performance of subject scores computed for dynamic acquisitions of varying length over the initial 10 min (Supplemental Table 3; Tables 2 and 3).

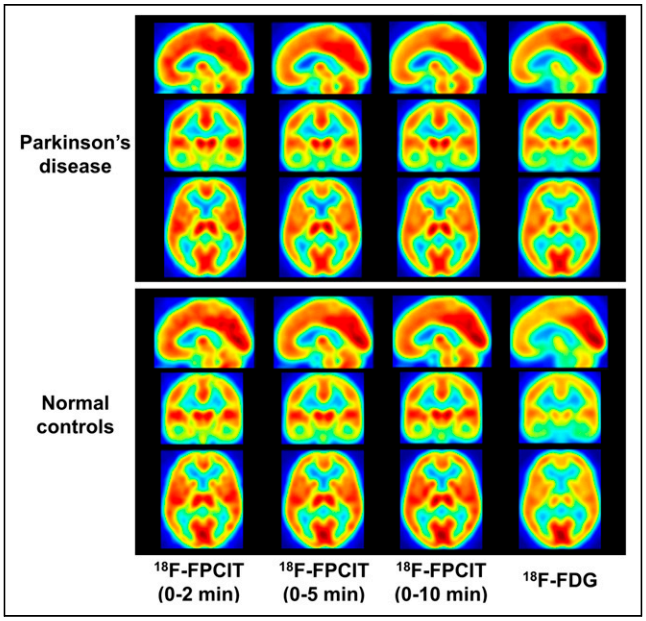

FIGURE 1. Mean images of PD patients and HCs from early-phase ^{18}F-FPCIT and ^{18}F-FDG PET after spatial normalization into a standard brain space. There was high similarity between mean ^{18}F-FPCIT images over first 2, 5, and 10 min after injection and corresponding ^{18}F-FDG images.

Disease Discrimination

Brain perfusion images from early-phase dynamic ^{18}F-FPCIT scans averaged over the first 2, 5, and 10 min after injection were similar to corresponding ^{18}F-FDG images in both PD patients and HC subjects (Fig. 1). The accuracy of group separation and longitudinal change for the various network expression measurements and for caudate or putamen DAT binding are summarized in Supplemental Table 3. Subject scores were elevated in the PD group, versus the HC group, for PDRP ($P < 0.04$, unpaired *t* tests) but not for PDCP ($P \geq 0.32$) in each of the 3 early-phase ^{18}F-FPCIT images (Figs. 2A and 2B). Subject scores in PD patients obtained with ^{18}F-FDG were also elevated for PDRP ($P < 0.02$) but did not reach significance for PDCP ($P = 0.11$). Computed PDRP subject scores did not differ significantly among the 3 different early-phase ^{18}F-FPCIT time windows ($P = 0.82$; 1-way repeated-measures ANOVA). No significant differences were seen between early-phase ^{18}F-FPCIT subject scores for each time window and the corresponding ^{18}F-FDG PET measures ($P \geq 0.15$; paired *t* tests). Differences in corresponding PDCP values did not reach significance across time windows ($P = 0.12$; 1-way repeated-measures ANOVA) but were lower for each ^{18}F-FPCIT time window than for ^{18}F-FDG PET ($P < 0.025$; paired *t* tests). By contrast, striatal DAT binding (Fig. 2C) was reduced ($P < 0.001$, unpaired *t* tests) in the PD group, relative to the HC group, and did not differ between the left and right striatal regions in the patient and HC groups ($P \geq 0.15$, paired *t* tests). The reduction was greater from the caudate to the anterior and posterior axis of the putamen ($P < 0.0001$).

In summary, subject scores measured with dynamic ^{18}F-FPCIT PET between 0 and 10 min had increased sensitivity in discriminating groups by PDRP (PD vs. HC) and in detecting longitudinal changes by both PDRP and PDCP (4 y vs. baseline in PD), compared with the composite 2-min and 5-min early-phase scans (Supplemental Table 3). We therefore reported the remaining results on the basis of the composite 10-min frame.

Clinical Correlations

PD patients showed strong intercorrelations between clinical Hoehn and Yahr stage, Unified PD Rating Scale motor ratings, and disease duration ($r \geq 0.700$, $P < 0.0001$); age did not correlate with the other variables ($r \leq 0.28$, $P \geq 0.18$). Off-state Unified PD Rating Scale motor ratings in PD patients correlated with PDRP subject scores computed over the first 10 min after ^{18}F-FPCIT injection ($r = 0.439$, $P = 0.028$; Supplemental Fig. 2A), but the correlation with PDCP scores did not reach significance in the same time window ($r = 0.339$, $P = 0.10$; Supplemental Fig. 2C). Clinical motor ratings did not correlate with DAT binding measured for the caudate, the putamen, or the putamen subregions (Supplemental Table 4). Disease duration correlated with PDRP ($r = 0.409$, $P = 0.042$; Supplemental Fig. 2B) and PDCP ($r = 0.457$, $P = 0.022$; Supplemental Fig. 2D) subject scores computed for the 10-min frame and with putamen DAT binding ($r = -0.419$, $P = 0.037$; Supplemental Fig. 3).

Relationships Between ^{18}F-FPCIT and ^{18}F-FDG PET Imaging Markers

We found significant correlations between PDRP subject scores in PD measured by the 2 methods ($r = 0.863$, $P < 0.0001$; Fig. 3A);

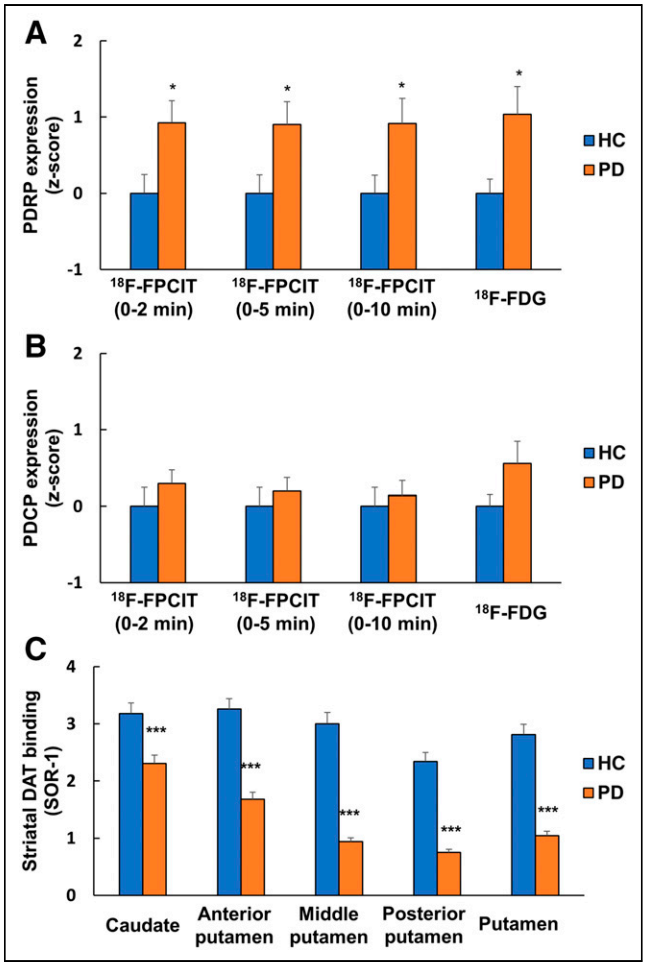

FIGURE 2. Differences in network scores and striatal DAT binding in PD patients compared with age-matched HC subjects. (A and B) Elevation in PDRP but not PDCP expression with pseudo-cerebral blood flow images from early-phase ^{18}F-FPCIT PET (0–2, 0–5, and 0–10 min) and metabolic images from ^{18}F-FDG PET. (C) Reduction in striatal DAT binding in caudate, putamen, and subdivisions of putamen from late-phase ^{18}F-FPCIT PET over 90–100 min. SOR = striatal-occipital ratio. *$P < 0.05$, unpaired Student *t* test. ***$P < 0.001$, unpaired Student *t* test.

analogous subject score correlations were also seen for PDCP ($r = 0.675$, $P < 0.005$; Fig. 3B). Moreover, within-modality correlations (Supplemental Table 5) were detected between PDRP and PDCP values measured with early-phase ^{18}F-FPCIT PET in PD patients ($r = 0.750$, $P < 0.0001$; Fig. 3C) and HC subjects ($r = 0.879$, $P < 0.00001$; Supplemental Fig. 4A) and with ^{18}F-FDG PET in PD patients ($r = 0.713$, $P = 0.001$; Supplemental Fig. 4B). In late-phase scans, DAT binding was significantly correlated for the caudate and putamen and across putamen subregions (PD: $r \geq 0.594$, $P \leq 0.002$; HC: $r \geq 0.931$, $P < 0.0001$; Supplemental Table 4). Nonetheless, caudate and putamen DAT binding correlations with PDRP subject scores computed in the early-phase scans were not significant ($|r| \leq 0.356$; $P \geq 0.10$; Table 2). However, PDCP expression computed in the early-phase scans exhibited a negative correlation (Table 3) with DAT binding in the caudate and the anterior putamen ($r = -0.404$, $P < 0.05$; Fig. 3D). By contrast, PDCP correlations with DAT binding measured in the whole putamen or in the middle and posterior putamen subregions did not reach significance ($|r| \leq 0.386$, $P \geq 0.06$).

Disease Progression

Brain perfusion images from early-phase dynamic ^{18}F-FPCIT scans were similar to corresponding ^{18}F-FDG images in PD at baseline and follow-up (Supplemental Fig. 5). Robust increases in Hoehn and Yahr clinical stages and motor ratings (Table 1) were recorded in the group of 8 PD patients who underwent longitudinal imaging over the 46-mo period ($P < 0.001$, paired *t* tests). The accuracy of longitudinal change for various network scores and for caudate and putamen DAT binding is presented in Supplemental Table 3. Expression levels for the both PDRP and PDCP increased (Figs. 4A, B, D, and E) over time in early-phase ^{18}F-FPCIT PET ($P < 0.01$ for each pattern), as well as in ^{18}F-FDG PET (PDRP: $P < 0.0005$; PDCP: $P < 0.02$; paired *t* tests). Conversely, the corresponding striatal DAT binding values in this PD subgroup decreased from baseline in both putamen and caudate nucleus ($P < 0.05$; Figs. 4C and 4F). Moreover, the rates of longitudinal changes did not significantly differ for PDRP and PDCP subject scores, or for putamen and caudate DAT binding, estimated, respectively, using early- and late-phase ^{18}F-FPCIT PET ($P > 0.10$, 2×2 repeated-measures ANOVA). By contrast, changes in subject scores were greater with ^{18}F-FDG PET than were the corresponding values obtained using early-phase ^{18}F-FPCIT PET, reaching significance for PDRP ($P = 0.004$) but not for PDCP ($P = 0.182$). The changes in subject scores were also greater for PDRP than for PDCP with ^{18}F-FDG PET ($P = 0.035$).

No correlations were detected between longitudinal changes in the imaging variables and motor ratings ($|r| \leq 0.362$, $P \geq 0.38$) or the between-scan interval ($|r| \leq 0.441$, $P \geq 0.27$). Interval changes demonstrated strong correlations in PDRP or PDCP subject scores between the 5-min and 10-min frames in early-phase ^{18}F-FPCIT ($r \geq 0.965$, $P < 0.0001$) and in striatal DAT binding values between putamen and caudate in late-phase ^{18}F-FPCIT ($r = 0.812$, $P = 0.014$). By contrast, significant correlations were not present between interval changes in PDRP and PDCP expression measured with early-phase ^{18}F-FPCIT or ^{18}F-FDG PET ($r \leq 0.536$, $P \geq 0.17$). Likewise, the changes recorded with the early-phase ^{18}F-FPCIT did not correlate with analogous changes in ^{18}F-FDG PET or with changes in striatal DAT binding recorded using the late-stage ^{18}F-FPCIT scans ($|r| \leq 0.482$, $P \geq 0.27$).

DISCUSSION

In this study, we found that PDRP expression levels measured in early-phase ^{18}F-FPCIT PET scans discriminated patients with early-stage PD from age-matched HC subjects with similar accuracy for the first 2, 5, and 10 min of the dynamic ^{18}F-FPCIT PET acquisitions. This level of discrimination was also detected using corresponding values obtained concurrently with ^{18}F-FDG PET in a smaller sample of PD and control subjects, as reported previously in similar early-stage PD cohorts (*25–28*). On the other hand, PDCP expression did not discriminate patients and HC subjects scanned with either ^{18}F-FPCIT or ^{18}F-FDG PET, consistent with the relatively intact cognitive function seen in these early-stage patients. That said, expression levels for both networks measured in early-stage PD patients with the early-phase ^{18}F-FPCIT images exhibited strong correlations with corresponding values from ^{18}F-FDG PET. Of note, the strength of these subject score correlations was comparable to that observed in PD patients scanned with both $H_2{}^{15}O$ and ^{18}F-FDG PET in the resting state (*5*,*17*) and in others who underwent dual-modality imaging with arterial spin labeling MRI and ^{18}F-FDG PET (*8*,*29*).

TABLE 2
Correlations Between Clinical Data and PDRP Scores or Striatal DAT Binding Values in PD Patients

Parameter	UPDRS	Duration	^{18}F-FPCIT over 0-2 min	^{18}F-FPCIT over 0-5 min	^{18}F-FPCIT over 0-10 min
PDRP score					
^{18}F-FPCIT over 0-2 min	0.423*	0.391			
^{18}F-FPCIT over 0-5 min	0.438*	0.407*	0.983†		
^{18}F-FPCIT over 0-10 min	0.439*	0.409*	0.954†	0.992†	
^{18}F-FDG			0.754†	0.837†	0.863†
Striatal DAT binding					
Caudate			−0.256	−0.290	−0.306
Putamen (whole)			−0.304	−0.301	−0.289
Anterior			−0.270	−0.273	−0.266
Middle			−0.356	−0.351	−0.342
Posterior			−0.319	−0.307	−0.297

*$P < 0.05$.
†$P < 0.0001$.
UPDRS = unified PD rating scale.
Data are Pearson correlation coefficients.

We also found that PDRP expression levels measured in early-stage PD patients using early-phase ^{18}F-FPCIT PET (2, 5, and 10 min) correlated with independent motor ratings, in keeping with previously published ^{18}F-FDG PET studies (*1*,*7*,*9*,*27*). Accordingly, analogous correlations with motor disability were not seen for PDCP subject scores computed in the same subjects (*1*,*11*,*30*). Along these lines, PDRP and PDCP expression levels computed in early-phase ^{18}F-FPCIT PET scans correlated with disease duration. Moreover, significant increases in these measures were seen over time in patients scanned longitudinally by this method, at rates comparable to those assessed using ^{18}F-FDG PET for network quantification (*16*). Nonetheless, given the small sample size, we were underpowered to detect any correlations between the changes in these brain network markers and clinical motor ratings.

On the other hand, symmetric and significant reductions in DAT binding were seen in the caudate and putamen, and in putamen subregions in late-phase ^{18}F-FPCIT PET scans from the same patients. In accord with prior studies, reductions in putamen DAT binding were seen with increasing disease duration (*31*). It is noteworthy that

TABLE 3
Correlations Between Clinical Data and PDCP Scores or Striatal DAT Binding Values in PD Patients

Parameter	UPDRS	Duration	^{18}F-FPCIT over 0-2 min	^{18}F-FPCIT over 0-5 min	^{18}F-FPCIT over 0-10 min
PDCP score					
^{18}F-FPCIT over 0-2 min	0.240	0.483*			
^{18}F-FPCIT over 0-5 min	0.318	0.483*	0.939†		
^{18}F-FPCIT over 0-10 min	0.339	0.457*	0.865†	0.983†	
^{18}F-FDG			0.510*	0.641‡	0.675‡
Striatal DAT binding					
Caudate			−0.446*	−0.430*	−0.404*
Putamen (whole)			−0.380	−0.345	−0.299
Anterior			−0.481*	−0.419*	−0.365
Middle			−0.386	−0.368	−0.334
Posterior			−0.264	−0.259	−0.237

*$P < 0.05$.
†$P < 0.0001$.
‡$P < 0.005$.
UPDRS = unified PD rating scale.
Data are Pearson correlation coefficients.

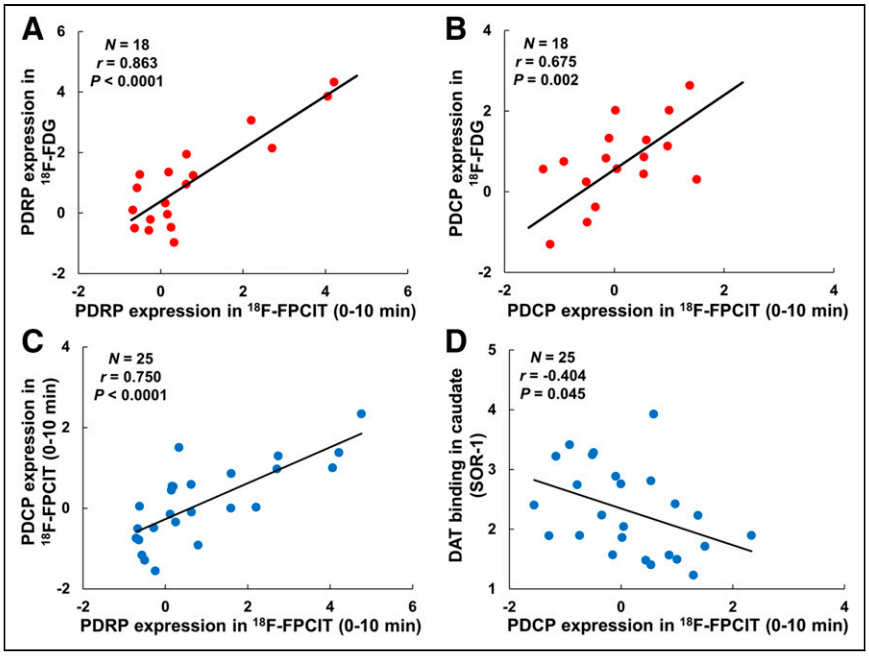

FIGURE 3. Correlations in network scores between surrogate cerebral blood flow images from early-phase ^{18}F-FPCIT and metabolic images in PD patients. (A and B) PDRP/PDCP expression computed using ^{18}F-FPCIT PET over 0–10 min correlated closely with that obtained with ^{18}F-FDG PET in same subjects (PDRP: $r = 0.863$, $P < 0.0001$; PDCP: $r = 0.675$, $P < 0.005$; Pearson correlations). (C and D) Corresponding PDCP expression correlated with PDRP expression ($r = 0.750$, $P < 0.0001$) and DAT binding in caudate ($r = -0.404$, $P < 0.05$). SOR = striatal-occipital ratio.

individual differences in caudate and anterior putamen DAT binding correlated with PDCP (but not PDRP) expression levels measured in the early-phase ^{18}F-FPCIT PET scans. This correlation underscores the role of these regions in mediating cognitive dysfunction in nondemented PD patients (*12*,*15*,*32*). That said, significant correlations were not observed between PDRP expression and putamen DAT binding. This lack of correlation was likely attributable to the lower signal and incipient floor effects noted in this region even in early-stage PD patients (*14*,*33*). Although caudate and putamen DAT binding declined significantly over the 4-y longitudinal study, the changes were small compared with the increases in PDRP and PDCP expression seen concurrently in the same subjects. This difference and the relatively small sample size may account for the absence of correlations between interval changes in the imaging measures.

PDRP and PDCP expression can be reliably quantified in early-phase ^{18}F-FPCIT PET scan data using computational methods similar to those used with ^{18}F-FDG PET. Indeed, the early-phase measurements were quite stable in discriminating early-stage PD from HC subjects and in assessing longitudinal changes in scans acquired over the initial 10 min after injection (Supplemental Tables 1–2). Likewise, correlations of PDRP and PDCP subject scores with motor ratings and disease duration, and with corresponding ^{18}F-FDG PET measurements, were maintained over each of the 1-min frames. Indeed, these findings are consistent with the performance of the composite frames obtained over the first 2, 5, and 10 min after injection.

Our results further indicate that early-phase ^{18}F-FPCIT PET images recorded over the first 10 min are superior for assessing PDRP and PDCP expression in individual patients. This superiority is likely due to the higher signal-to-noise ratio inherent in the long-time-frame images. Indeed, these scans exhibited stronger correlations with corresponding expression values from ^{18}F-FDG PET, as well as with Unified PD Rating Scale motor ratings (Tables 2–3; Fig. 3; Supplemental Fig. 2). In this regard, the findings are in line with previously reported regional data (*22*). Moreover, the 10-min time window provided useful network measurements even after omitting the first 1, 2, or even 5 min of the acquisition (Supplemental Tables 6–8).

It has been reported that the early-phase data of many specific PET radioligands mimic brain perfusion in healthy subjects and in patients with neurodegenerative disorders. This report has been validated in PET imaging studies of Alzheimer disease (*34*,*35*). Early-phase data from dopaminergic PET tracers such as ^{18}F-FDOPA (*15*), ^{11}C-raclopride (*20*), or DAT tracers such as ^{11}C-PE2I (*21*) can similarly be used to compute PDRP and PDCP expression in individual subjects. Dual-phase imaging with these tracers may offer the advantage of network quantification and dopaminergic assessments in a single PET session.

This study was limited in several ways. Because only a portion of the current sample was imaged with both tracers, we were unable to rigorously compare the early- and late-phase ^{18}F-FPCIT measurements with ^{18}F-FDG PET subject scores from the same individuals. Although PDRP scores in the early-phase ^{18}F-FPCIT data were comparable to ^{18}F-FDG PET, analogous PDCP scores from ^{18}F-FPCIT tended to be somewhat lower, particularly when the frames were integrated over a longer duration. Whether ^{18}F-FDG PET is more sensitive to gauging PDCP expression than is ^{18}F-FPCIT PET remains to be investigated by assessing the strength and reliability of their neuropsychologic correlates in PD patients with cognitive dysfunction. That said, PDRP and PDCP subject scores computed in early-phase ^{18}F-FPCIT PET scans replicated the findings in PD reported in many prior studies on this topic with ^{18}F-FDG PET.

The use of dynamic ^{18}F-FPCIT PET may help in the evaluation of antiparkinsonian treatments in which nigrostriatal dopamine function is improved along with downstream changes in disease networks such as PDRP. For example, in an ^{18}F-FDG PET study of retinal pigmented epithelial cells implanted in the putamen of parkinsonian nonhuman primates, we found that expression levels for the parkinsonism-related pattern (homologous to the PDRP in human PD) (*36*,*37*) were reduced by treatment (*38*). Conceivably, this change can be captured using early-phase ^{18}F-FPCIT PET while quantifying potential changes in dopaminergic innervation through late-phase imaging. Whereas cell-based interventions such as retinal pigmented epithelial cell implantation will not necessarily alter striatal DAT binding, dynamic ^{18}F-FPCIT PET may be appropriate for disease-modifying interventions such as the induction of growth factors in the putamen (*39*). Moreover, concurrent measurements of disease network expression in early-phase data can improve the accuracy of differential diagnosis based on clinical assessments with or without adjunctive dopaminergic imaging (*10*,*40*–*42*).

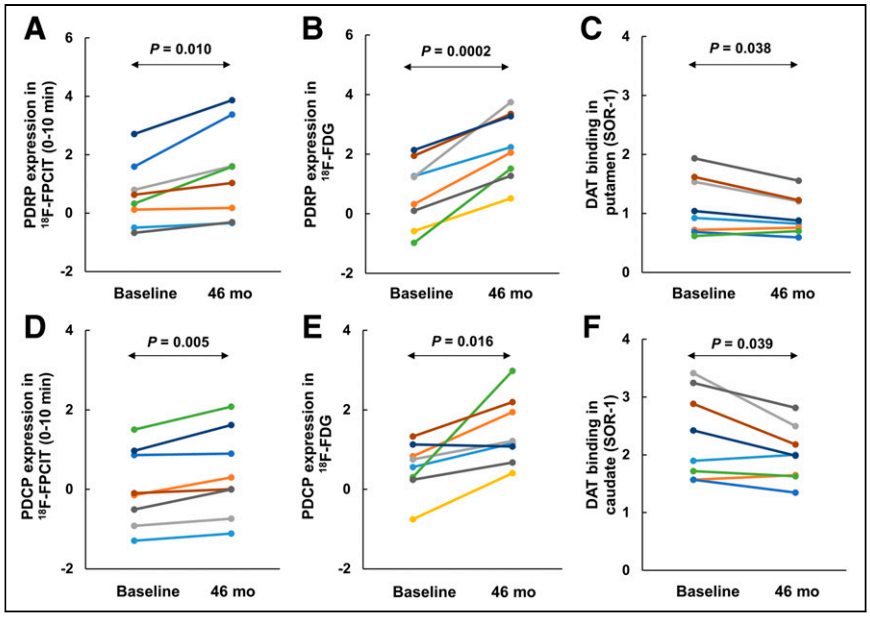

FIGURE 4. Longitudinal changes in network scores and striatal DAT binding in PD patients who underwent repeat PET imaging with both ^{18}F-FPCIT and ^{18}F-FDG. (A, B, D, and E) Increases in PDRP and PDCP expression ($P < 0.02$, paired Student *t* tests) with proxy cerebral blood flow images from early-phase ^{18}F-FPCIT PET over 0–10 min and metabolic images. (C and F) Reduction in striatal DAT binding ($P < 0.05$) in putamen and caudate from late-phase ^{18}F-FPCIT PET over 90–100 min. (Color codes are same for 7 PD subjects with dual-tracer data, with different colors for 2 other subjects with either ^{18}F-FPCIT or ^{18}F-FDG PET.) SOR = striatal-occipital ratio.

This hybrid approach may be especially useful in screening potential participants in trials of new interventions for PD and related disorders.

We emphasize that in this study, early-phase ^{18}F-FPCIT PET scans were used solely to quantify expression levels for the 2 validated disease-related metabolic networks, namely PDRP and PDCP. We did not interrogate other patient populations to see whether early-phase dynamic acquisitions appropriately captured other disease-related covariance patterns such as those reported previously for multiple-system atrophy, progressive supranuclear palsy, and corticobasal degeneration (*43*,*44*). It is also worth noting that although regional and network-level measurements of cerebral blood flow and glucose metabolism are coupled in healthy subjects and in early-stage PD patients scanned off medication, significant dissociation between these measures occurs during dopaminergic treatment (*18*,*19*). Uncoupling effects of this sort are particularly prominent in brain regions such as the putamen in which dopaminergic afferents are present to both neurons and blood vessels (*45*). Lastly, network approaches have recently been used to map specific treatment-induced metabolic patterns for investigational purposes (*46*). It is unclear at present, however, whether early-phase scans have sufficient power to capture stable network topographies of this sort. Further studies with both tracers will be needed to address these issues.

CONCLUSION

Dual-phase ^{18}F-FPCIT PET is a viable methodology for quantitative assessment of PD-related metabolic brain networks and presynaptic nigrostriatal dopaminergic functioning in a single imaging session. The ability to measure PDRP and PDCP expression levels and caudate and putamen DAT binding in individual patients after the injection of a single radiotracer represents a substantial saving in time and cost and is more convenient for patients.

DISCLOSURE

David Eidelberg serves on the scientific advisory board and has received honoraria from The Michael J. Fox Foundation for Parkinson's Research; serves on the scientific advisory board and receives personal fees from Ovid Therapeutics; has received consultant fees from MeiraGTx; is listed as a coinventor on patents regarding markers for use in screening patients for nervous system dysfunction and a method and apparatus for using the same, without financial gain; and has received research support from the NIH (NINDS NIDCD, and NIAID) and the Dana Foundation. This work was supported by the U.S. National Institute of Neurological Disorders and Stroke (P50 NS 071675 [Morris K. Udall Centre of Excellence for Parkinson's Disease Research at The Feinstein Institutes for Medical Research] to David Eidelberg). The content is solely the responsibility of the authors and does not necessarily represent the official views of the National Institutes of Health or the National Institute of Neurological Disorders and Stroke. No other potential conflict of interest relevant to this article was reported.

ACKNOWLEDGMENT

We thank Yoon Young Choi for her valuable editorial assistance preparing the manuscript.

KEY POINTS

QUESTION: Can the subject expression scores of disease-related brain networks be measured in early-phase dynamic ^{18}F-FPCIT PET images used to assess striatal DAT binding, and how do these measures compare with analogous network scores obtained with currently acquired ^{18}F-FDG PET scans and clinical indicators of disease severity and duration?

PERTINENT FINDINGS: The PDRP scores from ^{18}F-FPCIT correlated with the severity of clinical motor symptoms, whereas both PDRP and PDCP scores correlated with disease duration and more strongly with analogous brain network scores from ^{18}F-FDG in the same patients. The PDCP scores from ^{18}F-FPCIT data also correlated with DAT binding in caudate/anterior putamen, and the corresponding PDRP and PDCP scores from both early-phase ^{18}F-FPCIT and ^{18}F-FDG images increased with striatal DAT binding and further decreased from baseline in a subset of PD patients with follow-up.

IMPLICATIONS FOR PATIENT CARE: The method can be used to improve the outcomes of patient care and clinical research studies by increasing throughput in nuclear medicine centers with minimum radiation exposure and by more fully characterizing neuropathophysiology and evaluating disease discrimination and progression in parkinsonism.

REFERENCES

1. Eidelberg D. Metabolic brain networks in neurodegenerative disorders: a functional imaging approach. *Trends Neurosci.* 2009;32:548–557.
2. Spetsieris PG, Eidelberg D. Scaled subprofile modeling of resting state imaging data in Parkinson's disease: methodological issues. *Neuroimage.* 2011;54:2899–2914.
3. Peng S, Eidelberg D, Ma Y. Brain network markers of abnormal cerebral glucose metabolism and blood flow in Parkinson's disease. *Neurosci Bull.* 2014;30:823–837.
4. Schindlbeck KA, Eidelberg D. Network imaging biomarkers: insights and clinical applications in Parkinson's disease. *Lancet Neurol.* 2018;17:629–640.
5. Ma Y, Tang C, Spetsieris PG, Dhawan V, Eidelberg D. Abnormal metabolic network activity in Parkinson's disease: test-retest reproducibility. *J Cereb Blood Flow Metab.* 2007;27:597–605.
6. Huang C, Mattis P, Tang C, Perrine K, Carbon M, Eidelberg D. Metabolic brain networks associated with cognitive function in Parkinson's disease. *Neuroimage.* 2007;34:714–723.
7. Wu P, Wang J, Peng S, et al. Metabolic brain network in the Chinese patients with Parkinson's disease based on ^{18}F-FDG PET imaging. *Parkinsonism Relat Disord.* 2013;19:622–627.
8. Teune LK, Renken RJ, de Jong BM, et al. Parkinson's disease-related perfusion and glucose metabolic brain patterns identified with PCASL-MRI and FDG-PET imaging. *Neuroimage Clin.* 2014;5:240–244.
9. Tomše P, Jensterle L, Grmek M, et al. Abnormal metabolic brain network associated with Parkinson's disease: replication on a new European sample. *Neuroradiology.* 2017;59:507–515.
10. Ko JH, Lee CS, Eidelberg D. Metabolic network expression in parkinsonism: clinical and dopaminergic correlations. *J Cereb Blood Flow Metab.* 2017;37:683–693.
11. Meles SK, Tang CC, Teune LK, et al. Abnormal metabolic pattern associated with cognitive impairment in Parkinson's disease: a validation study. *J Cereb Blood Flow Metab.* 2015;35:1478–1484.
12. Niethammer M, Tang CC, Ma Y, et al. Parkinson's disease cognitive network correlates with caudate dopamine. *Neuroimage.* 2013;78:204–209.
13. Liu FT, Ge JJ, Wu JJ, et al. Clinical, dopaminergic, and metabolic correlations in Parkinson disease: a dual-tracer PET study. *Clin Nucl Med.* 2018;43:562–571.
14. Huang C, Tang C, Feigin A, et al. Changes in network activity with the progression of Parkinson's disease. *Brain.* 2007;130:1834–1846.
15. Holtbernd F, Ma Y, Peng S, et al. Dopaminergic correlates of metabolic network activity in Parkinson's disease. *Hum Brain Mapp.* 2015;36:3575–3585.
16. Niethammer M, Eidelberg D. Metabolic brain networks in translational neurology: concepts and applications. *Ann Neurol.* 2012;72:635–647.
17. Ma Y, Eidelberg D. Functional imaging of cerebral blood flow and glucose metabolism in Parkinson's disease and Huntington's disease. *Mol Imaging Biol.* 2007;9:223–233.
18. Hirano S, Asanuma K, Ma Y, et al. Dissociation of metabolic and neurovascular responses to levodopa in the treatment of Parkinson's disease. *J Neurosci.* 2008;28:4201–4209.
19. Jourdain VA, Tang CC, Holtbernd F, et al. Flow-metabolism dissociation in the pathogenesis of levodopa-induced dyskinesia. *JCI Insight.* 2016;1:e86615.
20. Van Laere K, Clerinx K, D'Hondt E, de Groot T, Vandenberghe W. Combined striatal binding and cerebral influx analysis of dynamic ^{11}C-raclopride PET improves early differentiation between multiple-system atrophy and Parkinson disease. *J Nucl Med.* 2010;51:588–595.
21. Appel L, Jonasson M, Danfors T, et al. Use of ^{11}C-PE2I PET in differential diagnosis of parkinsonian disorders. *J Nucl Med.* 2015;56:234–242.
22. Jin S, Oh M, Oh SJ, et al. Additional value of early-phase ^{18}F-FP-CIT PET image for differential diagnosis of atypical parkinsonism. *Clin Nucl Med.* 2017;42:e80–e87.
23. Ma Y, Dhawan V, Mentis M, Chaly T, Spetsieris PG, Eidelberg D. Parametric mapping of [^{18}F]FPCIT binding in early stage Parkinson's disease: a PET study. *Synapse.* 2002;45:125–133.
24. Peng S, Ma Y, Spetsieris PG, et al. Characterization of disease-related covariance topographies with SSMPCA toolbox: effects of spatial normalization and PET scanners. *Hum Brain Mapp.* 2014;35:1801–1814.
25. Matthews DC, Lerman H, Lukic A, et al. FDG PET Parkinson's disease-related pattern as a biomarker for clinical trials in early stage disease. *Neuroimage Clin.* 2018;20:572–579.
26. Meles SK, Renken RJ, Pagani M, et al. Abnormal pattern of brain glucose metabolism in Parkinson's disease: replication in three European cohorts. *Eur J Nucl Med Mol Imaging.* 2020;47:437–450.
27. Schindlbeck KA, Lucas-Jimenez O, Tang CC, et al. Metabolic network abnormalities in drug-naive Parkinson's disease. *Mov Disord.* 2020;35:587–594.
28. Tang CC, Holtbernd F, Ma Y, et al. Hemispheric network expression in Parkinson's disease: relationship to dopaminergic asymmetries. *J Parkinsons Dis.* 2020;10:1737–1749.
29. Ma Y, Huang C, Dyke JP, et al. Parkinson's disease spatial covariance pattern: noninvasive quantification with perfusion MRI. *J Cereb Blood Flow Metab.* 2010;30:505–509.
30. Mattis PJ, Niethammer M, Sako W, et al. Distinct brain networks underlie cognitive dysfunction in PD and AD. *Neurology.* 2016;87:1925–1933.
31. Benamer HT, Patterson J, Wyper DJ, Hadley DM, Macphee GJ, Grosset DG. Correlation of Parkinson's disease severity and duration with ^{123}I-FP-CIT SPECT striatal uptake. *Mov Disord.* 2000;15:692–698.
32. Carbon M, Ma Y, Barnes A, et al. Caudate nucleus: influence of dopaminergic input on sequence learning and brain activation in Parkinsonism. *Neuroimage.* 2004;21:1497–1507.
33. Nandhagopal R, Kuramoto L, Schulzer M, et al. Longitudinal progression of sporadic Parkinson's disease: a multi-tracer positron emission tomography study. *Brain.* 2009;132:2970–2979.
34. Lopes Alves I, Collij LE, Altomare D, et al. Quantitative amyloid PET in Alzheimer's disease: the AMYPAD prognostic and natural history study. *Alzheimers Dement.* 2020;16:750–758.
35. Beyer L, Nitschmann A, Barthel H, et al. Early-phase [^{18}F]PI-2620 tau-PET imaging as a surrogate marker of neuronal injury. *Eur J Nucl Med Mol Imaging.* 2020;47:2911–2922.
36. Ma Y, Peng S, Spetsieris PG, Sossi V, Eidelberg D, Doudet DJ. Abnormal metabolic brain networks in a nonhuman primate model of parkinsonism. *J Cereb Blood Flow Metab.* 2012;32:633–642.
37. Ma Y, Johnston TH, Peng S, et al. Reproducibility of a Parkinsonism-related metabolic brain network in non-human primates: a descriptive pilot study with FDG PET. *Mov Disord.* 2015;30:1283–1288.
38. Peng S, Ma Y, Flores J, et al. Modulation of abnormal metabolic brain networks by experimental therapies in a nonhuman primate model of Parkinson disease: an application to human retinal pigment epithelial cell implantation. *J Nucl Med.* 2016;57:1591–1598.
39. Whone A, Luz M, Boca M, et al. Randomized trial of intermittent intraputamenal glial cell line-derived neurotrophic factor in Parkinson's disease. *Brain.* 2019;142:512–525.
40. Rus T, Tomse P, Jensterle L, et al. Differential diagnosis of parkinsonian syndromes: a comparison of clinical and automated - metabolic brain patterns' based approach. *Eur J Nucl Med Mol Imaging.* 2020;47:2901–2910.
41. Tang CC, Poston KL, Eckert T, et al. Differential diagnosis of parkinsonism: a metabolic imaging study using pattern analysis. *Lancet Neurol.* 2010;9:149–158.
42. Tripathi M, Tang CC, Feigin A, et al. Automated differential diagnosis of early parkinsonism using metabolic brain networks: a validation study. *J Nucl Med.* 2016;57:60–66.
43. Eckert T, Van Laere K, Tang C, et al. Quantification of Parkinson's disease-related network expression with ECD SPECT. *Eur J Nucl Med Mol Imaging.* 2007;34:496–501.
44. Niethammer M, Tang CC, Feigin A, et al. A disease-specific metabolic brain network associated with corticobasal degeneration. *Brain.* 2014;137:3036–3046.
45. Lerner RP, Francardo V, Fujita K, et al. Levodopa-induced abnormal involuntary movements correlate with altered permeability of the blood-brain-barrier in the basal ganglia. *Sci Rep.* 2017;7:16005.
46. Niethammer M, Tang CC, Vo A, et al. Gene therapy reduces Parkinson's disease symptoms by reorganizing functional brain connectivity. *Sci Transl Med.* 2018;10:eaau0713.